Electronic Supplementary Material (ESI) for New Journal of Chemistry.

Supplementary information

Two-step electrosynthesis of nanocomposites of Ag, Au, Pd nanoparticles with iron(II) oxide-hydroxide

Rezeda R. Fazleeva, Gulnaz R. Nasretdinova, Aidar T. Gubaidullin, Vladimir G. Evtyugin, Vitaliy V. Yanilkin

Arbuzov Institute of Organic and Physical Chemistry, FRC Kazan Scientific Center, Russian Academy of Sciences, Arbuzov St. 8, 420088 Kazan, Russia

Experimental

2.3. Instrumentation

After completion of the electrolysis, the resulting solution was studied by CV, DLS, SEM, TEM, XRPD, UV-VIS, and IR spectroscopy and tested for catalytic activity.

For the study by SEM, TEM, DLS, UV-VIS, and IR spectroscopy, and XRPD, the nanocomposites obtained in the electrolyses were precipitated by centrifugation (14 500 rpm, 1 hour), were washed with solvent, which was used during the electrolysis (DMSO or DMSO-H_2O) and once with ethanol. The washing consisted of dispersing the precipitate in the solvent by sonication and subsequent precipitation by centrifugation (14 500 rpm, 1 hour).

UV-VIS.- Absorption spectra were recorded on a Perkin-Elmer Lambda 25 spectrometer (USA).

IR.- IR spectra were recorded for KBr pellets in the range of 4000–400 cm^{-1} on a Bruker Tensor 27 spectrometer (Germany) with an optical resolution of 4 cm^{-1} and an accumulation of 64 scans.

DLS.- The measurements were performed using a Malvern Instrument Zetasizer Nano (UK). The measured autocorrelation functions were analyzed with Malvern DTS software.

Electron microscopic analysis.- For SEM, the resulting solution was applied onto a titanium foil surface preliminarily cleaned by ultrasonic treatment in water, acetone, and ethanol. After that, the sample was dried at room temperature. In the case of TEM, 5 □l of the solution was placed on a 3 mm copper mesh with formvar/carbon (Formvar/Carbon, Lacey Formvar) support and dried at room temperature. After complete drying, the mesh in a special graphite holder was placed into a transmission electron microscope to perform the microanalysis.

The SEM studies were carried out using a Merlin field emission scanning electron microscope (Carl Zeiss, Germany). The surface morphology was imaged in the secondary electron (SE) mode with the primary electron accelerating voltage of 5 kV and with the probe current of 300 pA, to minimize the exposure to the object of study. To detect phase contrast, the accelerating voltage of primary electrons was 20 kV, and the probe current was 1 nA. The survey was carried out in the back-scattered electrons (AsB) mode. The microscope was equipped with an AZtec X-MAX energy dispersion spectrometer (Oxford Instruments, UK) with a resolution of 127 eV. The precision of measurement was 0.01-1%. The elemental analysis was carried out at the accelerating voltage of 20 keV and the flange focal length of 9.6 mm, which allowed minimizing the errors. The probing depth was less than 1 □m. In the quantitative analysis, a set of etalons incorporated into the Aztec program (reference standard for X-RAY microanalysis “Registered Standart No. 8842”) was used.

TEM-studies were carried out in the HR-TEM mode using a Hitachi HT 7700 Exalens (Japan) transmission electron microscope at the accelerating voltage of 100 keV with a resolution of 0.144 nm.

The elemental analysis was carried out using an Oxford Instruments X-Max^n 80T (UK) attachment equipped with a special holder.

XRPD.- The measurements were performed on a Bruker D8 Advance diffractometer equipped with Vario attachment and Vantec linear PSD, using Cu radiation (40 kV, 40 mA) monochromated by the curved Johansson monochromator (λ Cu $K_{\alpha 1}$ 1.5406 Å). Room-temperature data were collected in the reflection mode with a flat-plate sample.

The samples in liquid form were loaded on a silicon plate, which reduces background scattering. To increase the total amount of the sample, several more layers were applied on top of the first one after it dried. Patterns were recorded in the 2Θ range between 3° and 90°, in 0.008° steps, with a step time of 0.1–4.0s. Several diffraction patterns in various experimental modes and with different data accumulation times were collected and summed. The dried samples were scraped off the surface of the plate and, in the form of a powder, were replaced on a silicon plate to perform the verification experiment for the presence of preferential orientation of crystallites. To correct the angular position of peaks, additional experiments were performed with each sample with the addition of SRM676 corundum powder as an internal standard.

Processing of the obtained data was performed using EVA[1] and TOPAS[2] software packages. The crystallite size calculations were performed using the TOPAS software package in several ways: the values calculated from the half-width of the reflections (LVol-FWHM) and the integrated reflection intensity (LVol-IB) are the volume-weighted values of the crystallite sizes, and the CrySizeL parameter is the size of the crystallites in the direction perpendicular to the analyzed planes, with the Lorentz type of peak broadening. The minimization of the discrepancy between the experimental and calculated data in the refinement process was performed by the Rietveld method over the entire array of experimental data. Minimization in the process of the R_{wp} and R_{exp} convergence parameters verifying were used as a criterion of correct comparison of the calculated and experimental data. ICDD PDF-2 Release 2005 powder diffraction database was used for the identification of crystalline modifications.

References

1. *EVA v.11.0.0.3, User Manual*, SOCABIM, 2005.

2. *TOPAS V3, General profile and structure analysis software for powder diffraction data, Technical Reference*, Bruker AXS, Karlsruhe, Germany, 2005.

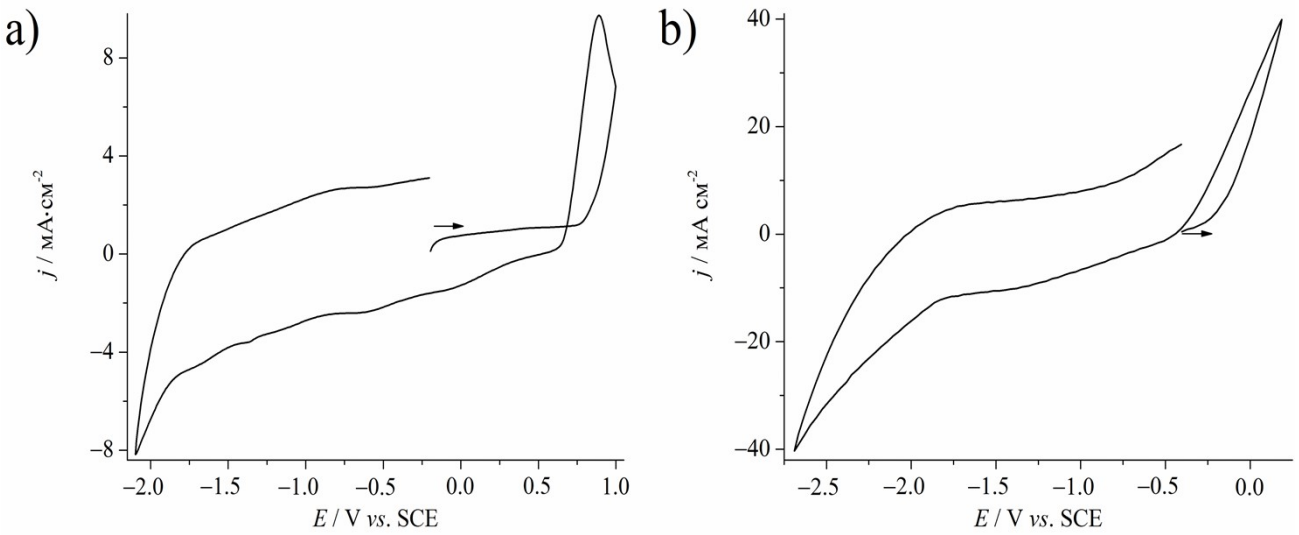

Fig. S1. CV of metal Fe^0 oxidation in the medium of DMF on the background of 0.1 M Bu_4NBF_4 (a) and Bu_4NCl (b). *v* = 100 mV/s.

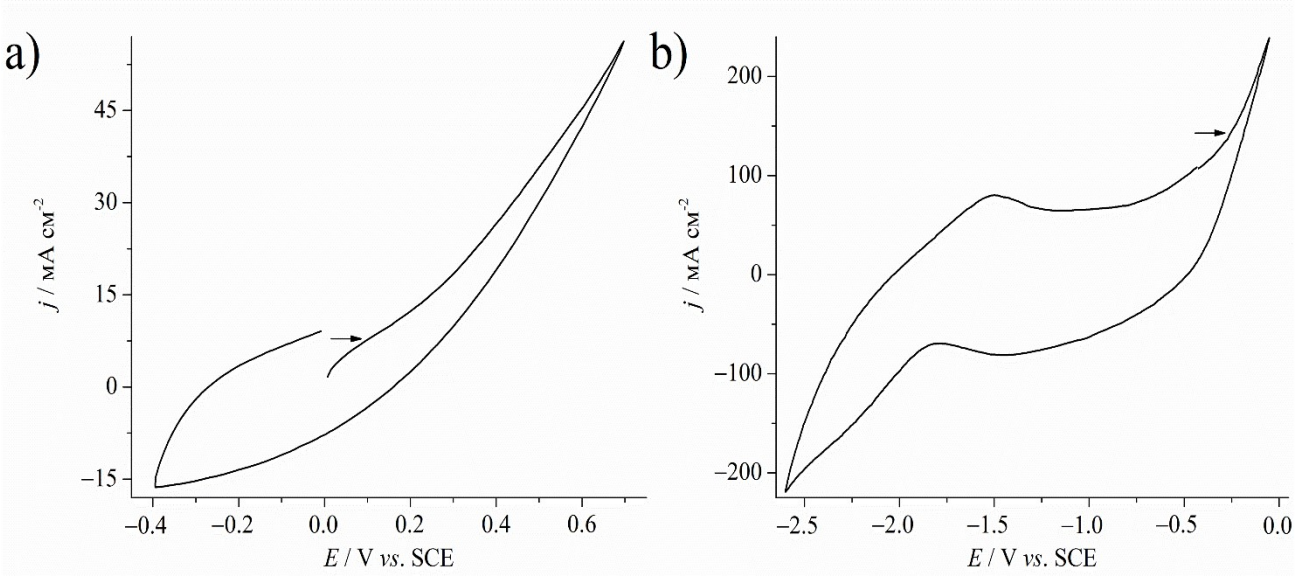

Fig. S2. CV of metal Fe^0 oxidation in the medium of AN on the background of 0.1 M Bu_4NBF_4 (a) and Bu_4NCl (b). *v* = 100 mV/s.

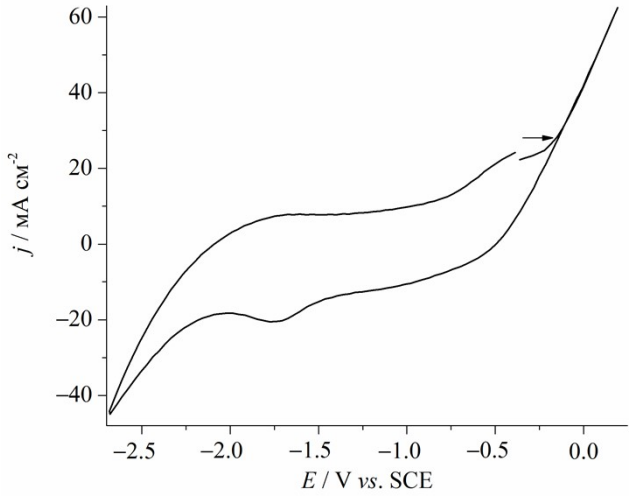

Fig. S3. CV of Fe^0 oxidation in the medium of DMSO on the background of 0.1 M Bu_4NCl. v = 100 mV/s.

Table S1. Conditions of the electrolyses with Fe-anode dissolution in solvents DMF, AN, and DMSO. The electrolysis temperature is 295 K.

№	Solvent	Supporting electrolyte, 0.1 M	$C_{Fe(II)}$[a] mM	C_{CTAC} mM	C_{PVP} mM	Parameters of the electrolysis			Fe-anode
						E, V *vs.* SCE	Q_r/Q_t[b], %	j[c], mA/cm^2	Changing of the weight, mg
1	DMF	Bu_4NBF_4	3	-	-	0.70	100	2.29	+7.5
2	DMF	Bu_4NCl	3	-	75	-0.10	35	2.39	+3.9
3	DMF	Bu_4NCl	3	75	-	-0.10	100	1.68	-1.1
4	AN	Bu_4NBF_4	3	-	-	0.70	100	2.90	+4.9
5	AN	Bu_4NBF_4	3	-	75	0.70	150	0.95	+6.3
6	AN	Bu_4NCl	3	-	-	-0.10	100	0.69	+2.0
7	DMSO	Bu_4NCl	3	-	-	-0.10	100	1.80	+8.8
8	DMSO	Bu_4NCl	3	75	-	-0.10	100	1.80	+10.8
9	DMSO	Bu_4NCl	1.5	-	-	-0.10	100	1.65	+5.4

[a] The target concentration of metal ions, which theoretically could be upon passing Q_t=2F with respect to mol of Fe(II). [b] The ratio of the real passed amount of electricity (Q_r) to theoretical Q_t; [c] Anodic current density.

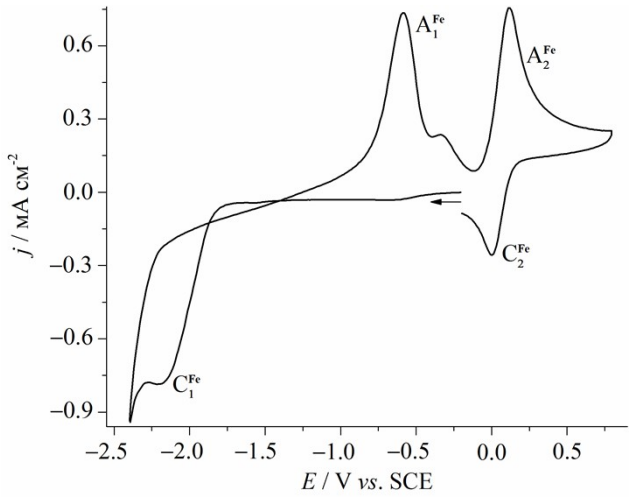

Fig. S4. CV of the solution after electrolysis with the dissolution of Fe-anode at E = -0.10 V (2F with respect to 3 mM Fe(II)) in the presence of 75 mM CTAC. DMF/0.1 M Bu_4NCl, v = 100 mV/s.

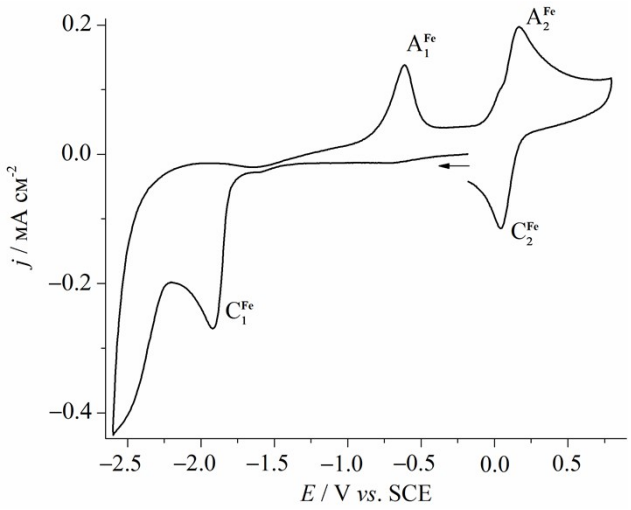

Fig. S5. CV of the solution after electrolysis with the dissolution of Fe-anode at *E* = -0.10 V (2F with respect to 1.5 mM Fe(II)). DMSO/0.1 M Bu_4NCl, *v* = 100 mV/s.

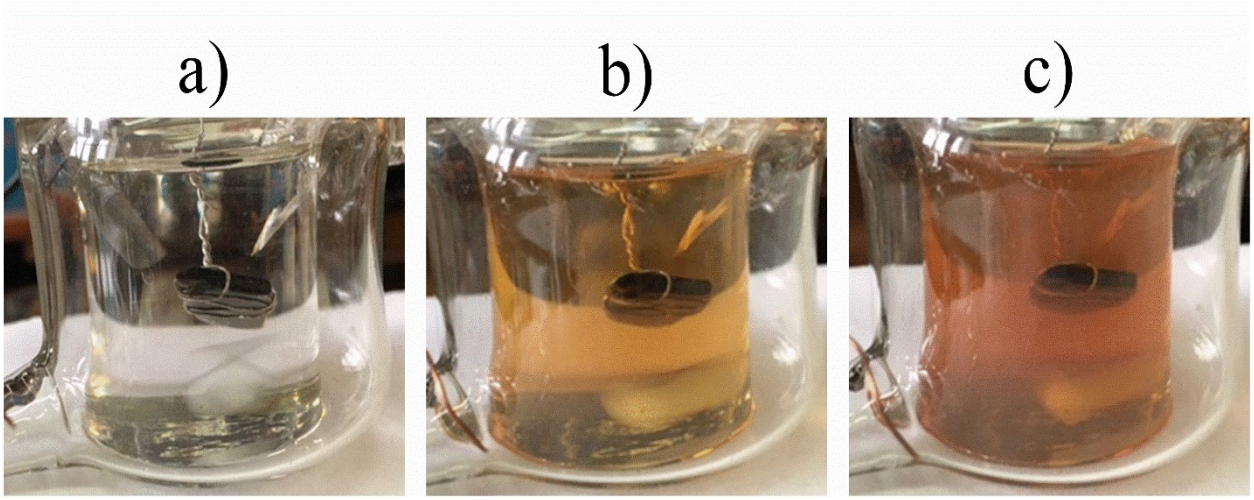

Figure S6. Photos of the electrolysis cell during the electrolysis with Fe-anode dissolution at the potential of $O_2^{\bullet-}$ generation *E* = -1.00 V in ДМСО/0.1 M Bu_4NCl medium after passing various amounts of electricity (2F with respect to 3 mM Fe(II)), %: 0 (a), 30 (b), 100 (c).

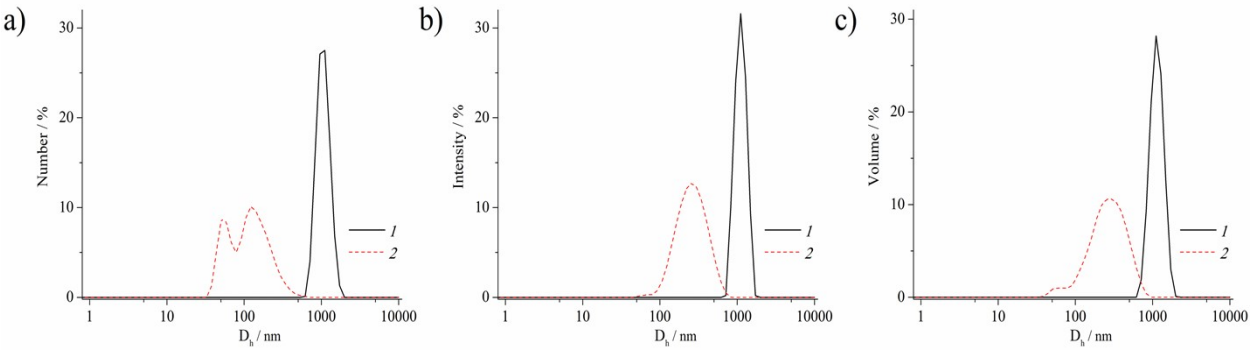

Fig. S7. Particle size distribution diagram (DLS) of FeO-x$Fe(OH)_2$ NPs by number (a), intensity (b), and volume (c) in the solution after electrolysis (*1*), isolated and dispersed in ethanol (*2*).

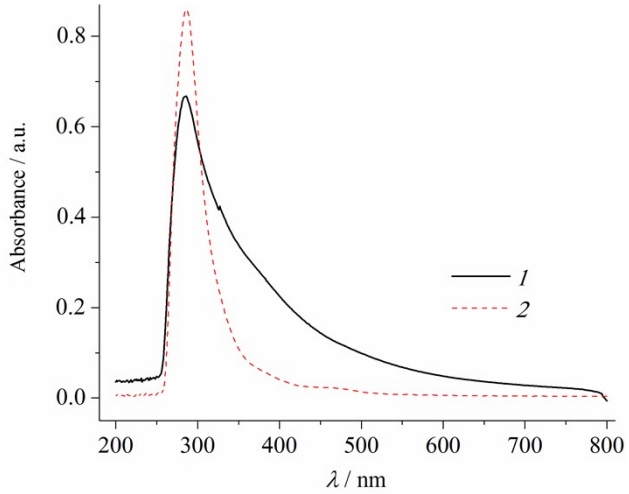

Fig. S8. UV-VIS spectra of FeO-xFe(OH)$_2$ in the solution after electrolysis (ДМСО) (*1*) and ethanol (*2*).

Table S2. The potentials (V *vs.* SCE) of reduction (E_C) and reoxidation (E_A) peaks and current densities of first reduction peaks (j_C^1) of investigated substrates on the GC electrode in DMSO(DMSO-H_2O(1:1))/0.1 M Bu_4NPF_6 (Bu_4NCl). ν = 100 mV/s.

Substrate	E_C, V	j_C^1, □A/cm^2	E_A, V
DMSO/0.1 M Bu_4NCl			
BQ	-0.38 -1.03,-1.25	0.19	-0.31 -0.86,-1.15
BQ + AgCl	-0.39 -1.28	0.22	-0.28 -0.81,-1.15
BQ + AuCl	0.03 -0.39 -1.25	0.03	-0.31 -0.88
DMSO/0.1 M Bu_4NPF_6			
MV^{2+}	-0.48 -0.84	0.21	-0.40 -0.75
MV^{2+} + Ag^+	0.09 -0.48 -0.80	0.20	0.29 -0.40 -0.76
DMSO-H_2O (1:1))/0.1 M Bu_4NCl			
MV^{2+}	-0.64 -0.98	0.25	-0.52 -0.88
MV^{2+} + AuCl	-0.28 -0.63 -0.98	0.07	0.76 -0.51 -0.88

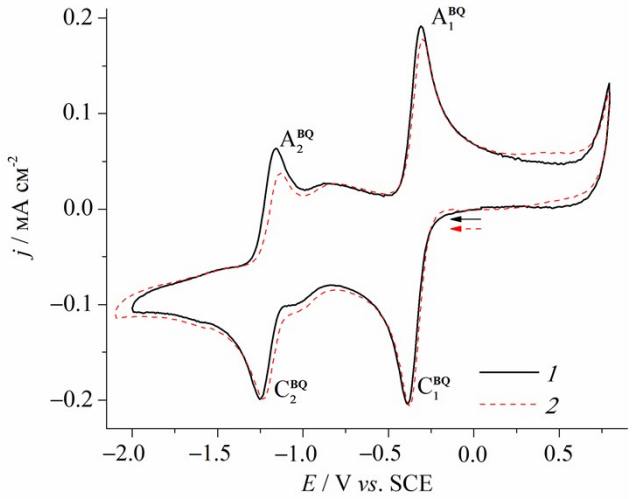

Fig. S9. CV of 2mM BQ in DMSO/0.1 M Bu_4NCl medium in the absence (*1*) and presence (*2*) of $FeO\text{-}xFe(OH)_2$. *v* = 100 mV/s

Table S3. Conditions of mediated electrosynthesis of MNPs (M = Ag, Au, and Pd) at the controlled potential *E* = -0.50 V in DMSO/0.1 M Bu_4NCl medium. $C_{M^{z+}}$ [a] = 1.5 mM, C_{BQ} = 2 mM, the synthesis temperature is 295 K.

№	Type of metal ions addition	Parameters of the electrolysis		Changing of the electrode weight, mg		Decrease in the BQ concentration, %
		Q_r/Q_t[b], %	J[c], mA/cm^2	M-anode	GC cahode	
1	AgCl	100	0.31→0.19	-	+1.1	50
2	AuCl	80	0.47→0	-	-	70
3	Pd-anode	21	0.16→0.04	-1.0	+2.1	60

[a] The target concentration of metal ions, in the case of Pd, which theoretically could be upon passing Q_t=2F with respect to mol of Pd(II). [b] The ratio of the real passed amount of electricity (Q_r) to theoretical Q_t; [c] Cathodic current density.

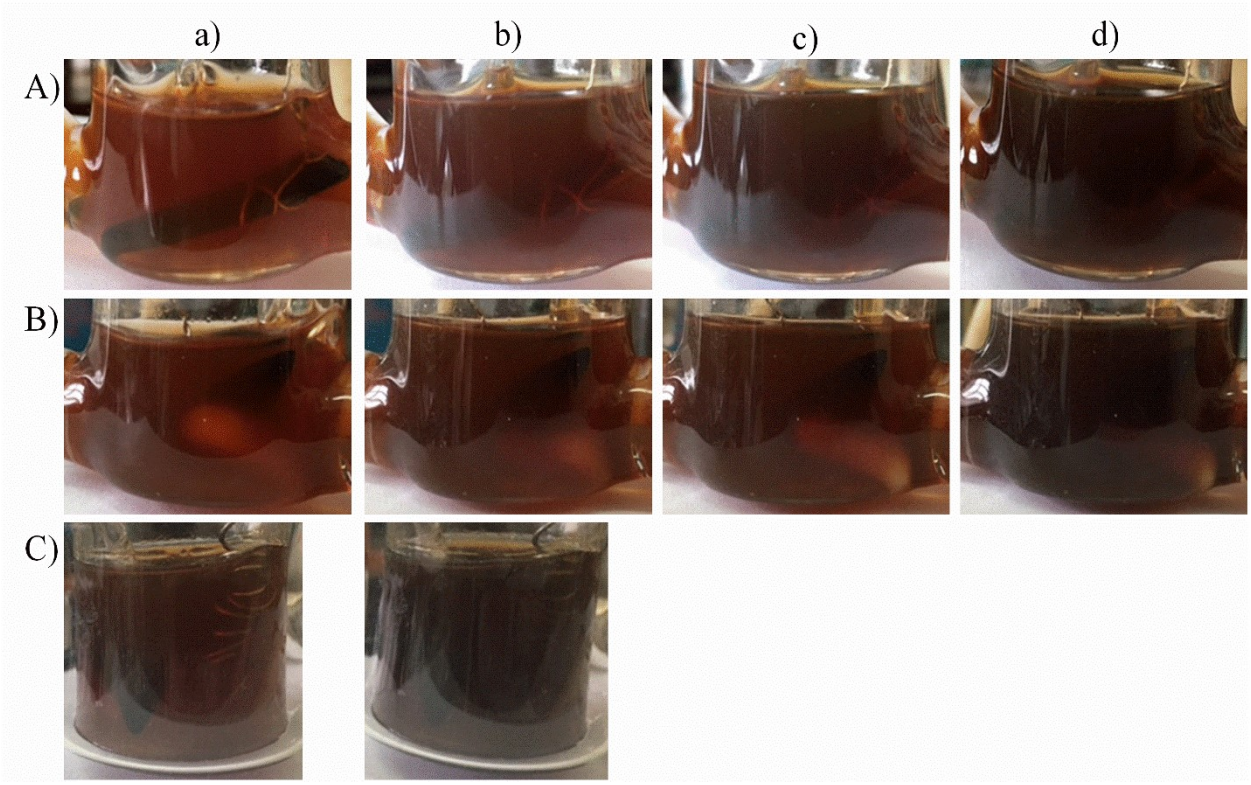

Fig. S10. Photos of the electrolysis cell during the electrolysis in 2mM BQ + 1.5 mM Ag(I) (A), (1.5 mM Au(I) (B) and 0.63 mM Pd(II) (C)) + 5.1 mM FeO-xFe(OH)$_2$ at the potential of $BQ^{\bullet-}$ generation E = -0.50 V in ДМСО/0.1 M Bu_4NCl medium after passing various amounts of electricity (1F with respect to 1.5 mM Ag(I), Au(I) and 2F with respect to 1.5 mM Pd(II)), %: 0 (a), 20 (b), 50 (c), 80 (Au), 100 (Ag) (d).

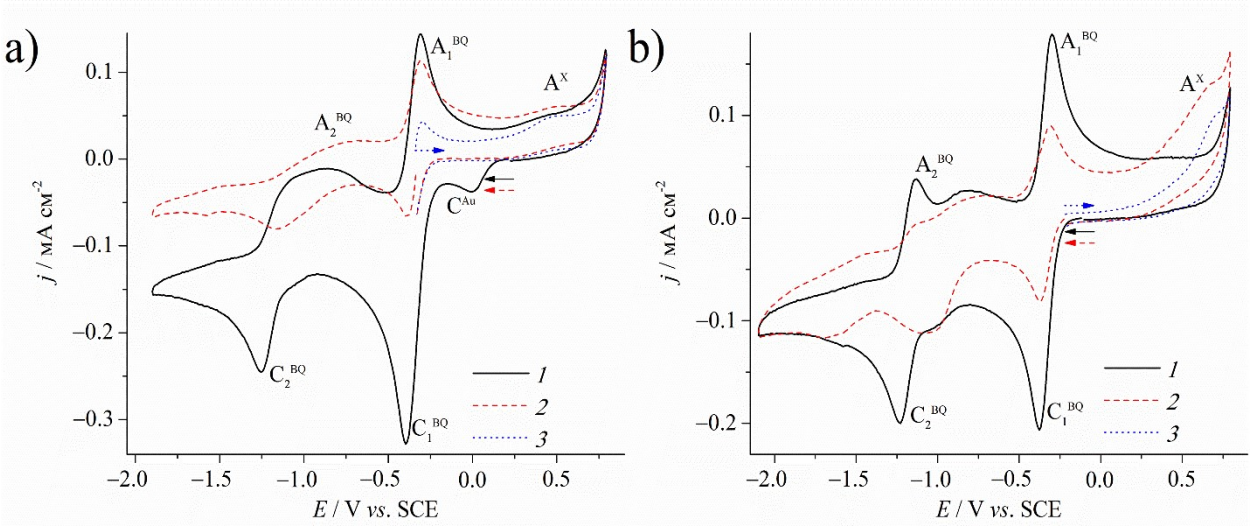

Fig. S11. CV of the (a) 2mM BQ + 1.5 mM AuCl + 5.1 mM FeO-xFe(OH)$_2$ and (b) 2mM BQ + Pd-anode + 5.1 mM FeO-xFe(OH)$_2$ systems in ДМСО/0.1 M Bu_4NCl before (*1*) and after electrolysis (*2, 3*). v = 100 mV/s

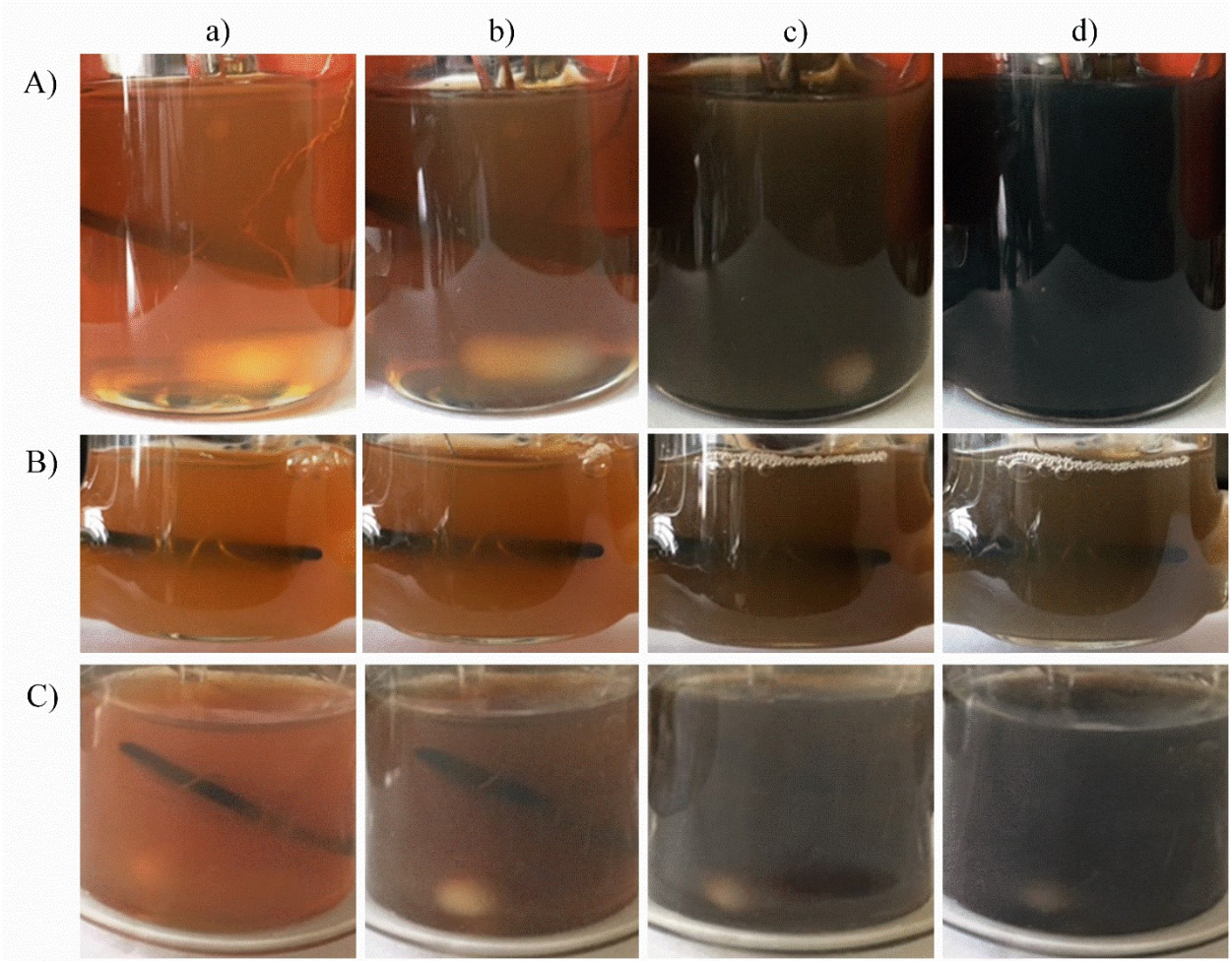

Fig. S12. Photos of the electrolysis cell during the electrolysis in 2mM MV^{2+} + 1.5 mM Ag(I) (A), (1.5 mM Au(I) (B) and 2.1 mM Pd(II) (C)) + 4.3 mM (A) and 5.1 mM (B, C) FeO-x$Fe(OH)_2$ at the potential of $MV^{\bullet+}$ generation E = -0.55 V (A) and E = -0.70 V (B, C) in DMSO/0.1 M Bu_4NPF_6 (A) and DMSO-H_2O(1:1)/0.1 M Bu_4NCl (B, C) media after passing various amounts of electricity (1F with respect to 1.5 mM Ag(I), Au(I) and 2F with respect to 1.5 mM Pd(II)), %: 0 (a), 30 (b), 70 (c), 100 (d).

Table S4. Lattice parameters, crystallite average sizes of samples Ag/FeO-x$Fe(OH)_2$, Au@CTAC/FeO-x$Fe(OH)_2$, and Pd@CTAC/FeO-x$Fe(OH)_2$.

Miller Indices	Ag/FeO-x$Fe(OH)_2$				Au@ CTAC/FeO-x$Fe(OH)_2$	Pd@ CTAC/FeO-x$Fe(OH)_2$	
	111	200	220	311	111	111	200
Angle 2θ, º	38.139(2)	44.249(12)	64.477(12)	77.390(13)	38.252(11)	39.64(1)	45.96(4)
CrySizeL (nm)	19.28(55)	10.82(97)	19.3(28)	16.4(21)	13.4(15)	5.1(2)	6.1(18)
LVol-IB (nm)	12.28(61)	9.89(96)	12.3(31)	10.5(22)	8.5(16)	3.3(2)	4.4(17)
Lvol-FWHM (nm)	17.17(59)	9.63(98)	17.2(30)	14.6(22)	11.9(15)	4.6(2)	4.6(15)
R_{wp}	3.18%.				2.77%	2.80%	
R_{exp}	2.87%				2.61%	2.59%	
GOF	1.11				1.06	1.08	

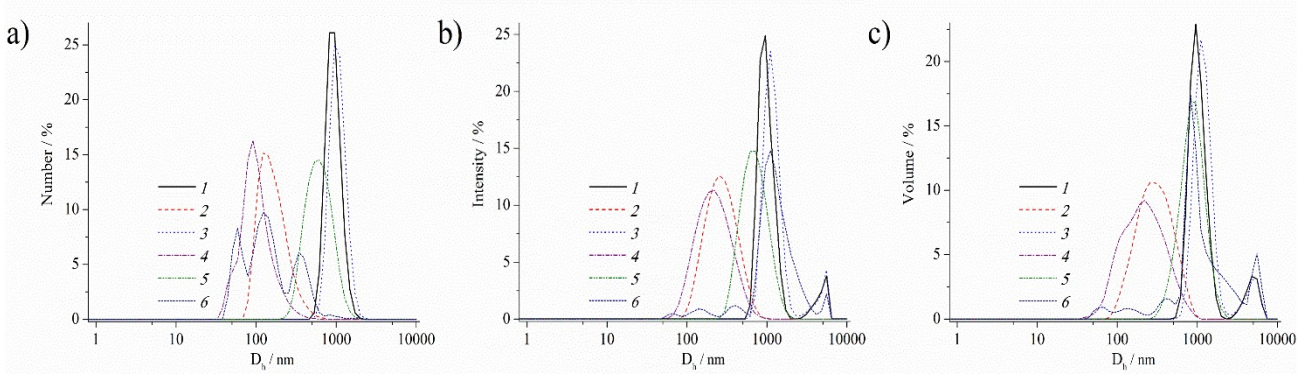

Fig. S13. Particle size distribution diagram (DLS) of Pd@CTAC/FeO-xFe(OH)$_2$ (*1,2*), Au@CTAC/FeO-xFe(OH)$_2$ (*3,4*) and Ag/FeO-xFe(OH)$_2$ (*5,6*) nanocomposites by number (a), intensity (b), and volume (c) in the solution after electrolysis (*1,3,5*), isolated and dispersed in ethanol (*2,4,6*).

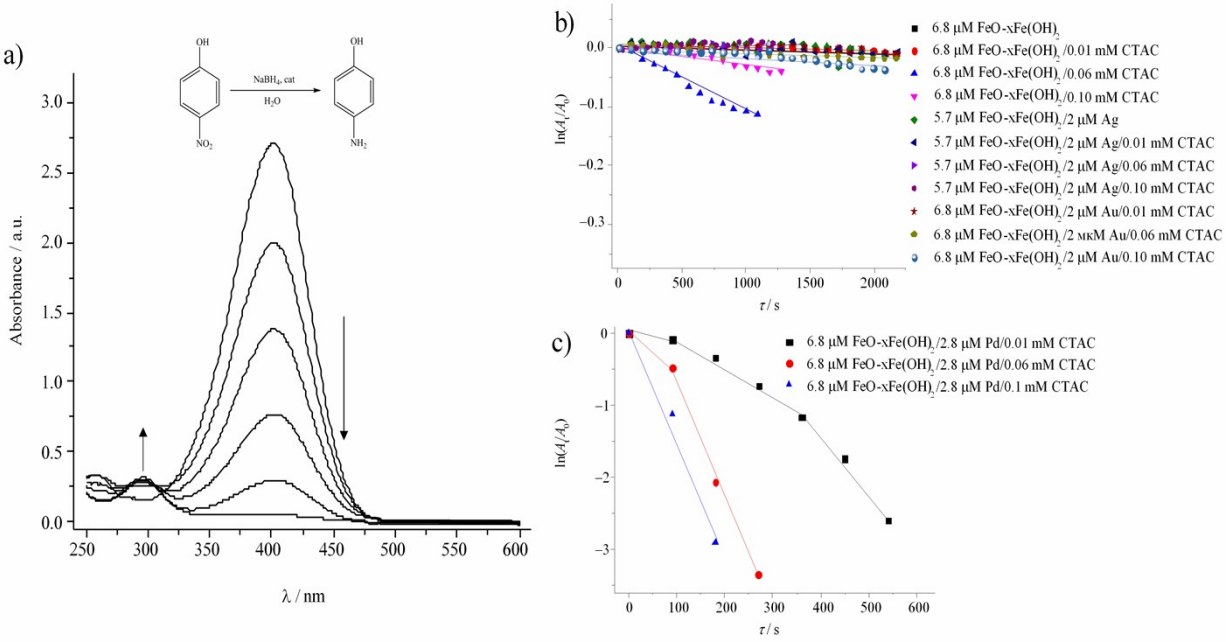

Fig. S14. Reduction of *p*-nitrophenol (0.1 mM) with sodium borohydride (5 mM) catalyzed by oxide-hydroxide FeO-xFe(OH)$_2$ and Ag/FeO-xFe(OH)$_2$, Au@CTAC/FeO-xFe(OH)$_2$, Pd@CTAC/FeO-xFe(OH)$_2$ nanocomposites in the absence and presence of CTAC: changes in the UV-VIS spectrum of the reaction mixture obtained after addition of catalyst Pd@CTAC/FeO-xFe(OH)$_2$ (a); semilogarithmic kinetic curve of oxide-hydroxide FeO-xFe(OH)$_2$ and Ag/FeO-xFe(OH)$_2$, Au@CTAC/FeO-xFe(OH)$_2$ nanocomposites (b) and of Pd@CTAC/FeO-xFe(OH)$_2$ nanocomposite upon the increase in CTAC concentration (c); where A_0 is the optical density before the addition of catalyst, A_t is the current optical density; H_2O, 25 ^oC.